# Simultaneous Global Localization and Mapping

Hyukdoo Choi, KwangWoong Yang, and Euntai Kim

***Abstract*—This paper proposes a hybrid approach to global localization and simultaneous localization and mapping (SLAM). Global localization and SLAM techniques have been independently developed but now researchers seek to simultaneously solve two problems regarding localization with an imperfect map and no a priori state information. Until now, integration of global localization and SLAM have not undergone extensive research. We propose a new approach for the new problem, called simultaneous global localization and mapping (SiGLAM). Our method is derived from the feature-driven method of global localization but evolved to be more robust to sensor noise and imperfections in a map. We do not wait until the only hypothesis survives. Hypotheses are continuously generated and managed in a conservative way. Instead, the best hypothesis is selected by hypothesis scoring. We demonstrate the proposed algorithm with simulations and real-world experiments. The results prove that our method outperforms other existing methods.**

***Index Terms*—Global localization, imperfect map, partially known map, simultaneous localization and mapping (SLAM).**

## I. Introduction

LOCALIZATION is a fundamental problem in mobile robotics. An easy solution is a GPS sensor aided by an inertial sensor [1] but GPS has a lot of blind spots such as indoor environment. In this situation, localization largely consists of three kinds of problems. A local localization problem occurs when both a map of the environment and a priori state information are given. If only a map is provided, this is a global localization problem. When only an a priori state is given, both states of the map and pose are estimated simultaneously, which is called simultaneous localization and mapping (SLAM) [2], [3]. For this reason global localization and SLAM have been considered disjointed problems. However, they are not disjointed in practice, especially when the given map is imperfect. An imperfect map has small errors between the map and the real environment and either a lack or an excess of landmarks. A perfect map fully describes every landmark in the target environment. Many localization solutions utilize floor plans, but a floor plan is an imperfect map. When only an imperfect map is given with no initial state, how can we achieve global localization? This paper considers this question.

We determined that in this situation, both global localization and SLAM problems have to be solved simultaneously and dependently. Let us call this problem simultaneous global localization and mapping (SiGLAM). This paper is presented to propose a solution to this problem.

There have been two main streams of global localization: the known correspondence approaches and the unknown correspondence approaches. Known correspondence approaches usually extract unique features from measurements, called "descriptors" [4]–[7]. If the scene of an environment is complex enough, global localization is solved by an instant match between current and previous descriptors [8]–[12]. Unknown correspondence approaches utilize structural features like lines and points and accumulate feature information until the history of the features becomes unique in the given map [13]–[18].

A popular implementation of an unknown correspondence approach is the feature-driven method [15]–[18]. This method detects the possible candidates of the true pose of a robot, called hypotheses, by matching current measurements with a given map. Then, it tracks the hypotheses and removes improbable ones. This method works effectively in a perfect map but its performance can deteriorate significantly due to small errors in the map.

Previous work focused on fast data association by using a tree structure. Those researches dealt with measurements that were not matched with a map as false alarms, but no one clearly stated how many false alarms can be tolerated for each hypothesis not to be considered as improbable and so not to be removed [15], [16]. If the hypothesis elimination condition is too strict, temporarily outlying measurements can void the true hypothesis, which is tracking the true pose of a robot. Conversely, a loose elimination condition lets too many hypotheses survive, which results in late localization.

The elimination condition should be carefully selected but it inevitably depends on the environment. Our approach is derived from the feature-driven method but evolved to handle false alarms. In our approach, we consider that false alarm measurements may come from unregistered landmarks out of the given map and apply the SLAM algorithm to fill up the vacancies in the given map, not removing any hypotheses. Once an unregistered landmark is incorporated into the SLAM map, the landmark makes no more harm to the hypothesis while the previous methods are badly affected whenever it meets unregistered landmarks. Since this approach is too conservative to eliminate false hypotheses, the hypotheses are scored. The earlier methods [17], [18] gave hypotheses marks based on measurement likelihoods, but the likelihoods are sensitive to sensor noise and not reliable, especially in a symmetric environment. On the contrary, the proposed method gives a quantized score by using

Manuscript received January 21, 2013; accepted June 11, 2013. Date of publication August 21, 2013; date of current version April 25, 2014. Recommended by Technical Editor S. Verma. This work was supported by the Basic Science Research Program through the National Research Foundation of Korea (NRF) funded by the Ministry of Education, Science and Technology (2013024001).

H. Choi and E. Kim are with the School of Electrical and Electronic Engineering, Yonsei University, Seoul 120-749, Korea (e-mail: goodgodgd@yonsei.ac.kr; etkim@yonsei.ac.kr).

K. W. Yang is with the Korea Institute of Industrial Technology (KITECH), Ansan 426-791, Korea (e-mail: page365@gmail.com).

Color versions of one or more of the figures in this paper are available online at http://ieeexplore.ieee.org.

Digital Object Identifier 10.1109/TMECH.2013.2274822

TABLE I
NOMENCLATURE OF THE SYSTEM

| Notations | Descriptions |
|---|---|
| $\mathbf{m} = \begin{bmatrix} m_P^{1:N_G} & m_L^{1:M_G} \end{bmatrix}$ | The total given map |
| $m_P^i = \begin{bmatrix} m_{Px}^i & m_{Py}^i \end{bmatrix}$ | Coordinates of the $i$ th point landmark in the given map |
| $m_L^i = \begin{bmatrix} m_{Ld}^i & m_{Lb}^i \end{bmatrix}$ | Distance and angle of the $i$ th line landmark in the given map |
| $\mathbf{s}_t = \begin{bmatrix} s_{P,t}^{N_G+1:N} & s_{L,t}^{M_G+1:M} \end{bmatrix}$ | The total SLAM map |
| $s_{P,t}^i = \begin{bmatrix} s_{Px,t}^i & s_{Py,t}^i \end{bmatrix}$ | Coordinates of the $i$ th point landmark in the SLAM map |
| $s_{L,t}^i = \begin{bmatrix} s_{Ld,t}^i & s_{Lb,t}^i \end{bmatrix}$ | Distance and angle of the $i$ th point landmark in the SLAM map |
| $N_G$ | The number of given point landmarks |
| $N_S$ | The number of SLAM point landmarks |
| $N = N_G + N_S$ | The number of total point landmarks |
| $M_G$ | The number of given line landmarks |
| $M_S$ | The number of SLAM line landmarks |
| $M = M_G + M_S$ | The number of total line landmarks |
| $\mathbf{x}_t = \begin{bmatrix} x_t & y_t & b_t \end{bmatrix}$ | The robot's pose |
| $\mathbf{y}_t = \begin{bmatrix} \mathbf{x}_t & \mathbf{s}_t \end{bmatrix}$ | The total state vector |
| $\mathbf{u}_t = \begin{bmatrix} v_t & w_t \end{bmatrix}$ | Linear and angular velocity |
| $\mathbf{z}_t = \begin{pmatrix} z_{P,t}^{1:n_P} & z_{L,t}^{1:n_L} \end{pmatrix}$ | Total point and line measurements |
| $\mathbf{c}_t = \begin{pmatrix} c_{P,t}^{1:n_P} & c_{L,t}^{1:n_L} \end{pmatrix}$ | Total correspondence variables |
| $n_p$ | The number of point measurements |
| $n_L$ | The number of line measurements |

the history of data association. A hypothesis is considered to be most credible when the hypothesis has detected more given landmarks and fewer unregistered landmarks than any other hypotheses. This policy makes the score almost invariant under small sensor noise.

This paper is organized as follows. The next section describes the problem and models the system with equations and parameters on which our formulation is based. Our SiGLAM algorithm is presented in Section III, explaining how hypotheses are generated, tracked, scored, and eliminated. Sections IV and V give the simulation and experimental results, respectively.

## II. Problem Statement

The problem treated in this paper is a global localization problem with an imperfect map. More specifically, the environment is structured by line and point landmarks in two dimensions. Some landmarks are provided within the given map but the rest remain unknown. Our goal is building an additional map of unregistered landmarks as well as localizing a robot with no initial state information. Since the additional map is built by the SLAM algorithm, it is called a SLAM map. Therefore, there are two kinds of maps, given and SLAM, and two kinds of landmarks, point and line, for each map. The notations regarding this problem are presented in Table I. The row vectors in Table I are actually column vectors, where transpose marks are omitted for simplicity.

In order to formalize our algorithm, we have to define the system models for the movement and perception of a robot. The detailed equations of the models are given in our previous work [19]. The robot's motion is ruled by the velocity motion model defined as follows:

$$\mathbf{x}_t = g(\mathbf{u}_t, \mathbf{y}_{t-1}) + N(\mathbf{0}, R) \tag{1}$$

where $\mathbf{u}_t = \begin{bmatrix} v_t & w_t \end{bmatrix}$ is a control input, containing a linear velocity $v_t$, and an angular velocity $w_t$, and $R$ is the noise covariance of the motion model. When a robot observes a point landmark, the relative distance and angle of the point is measured. However, the landmark variable can differ depending on whether the point is from the given map or from the SLAM map. Hence the point measurement model is separated with respect to the correspondence variable as follows:

$$\begin{aligned} &\text{If } k = c_{P,t}^j \le N_G \\ &z_{P,t}^j = \begin{bmatrix} z_{Pd,t}^j \\ z_{Pb,t}^j \end{bmatrix} = v_P\left(\mathbf{x}_t, m_P^k\right) + N(\mathbf{0}, Q_P) \\ &\text{else} \\ &z_{P,t}^j = \begin{bmatrix} z_{Pd,t}^j \\ z_{Pb,t}^j \end{bmatrix} = v_P\left(\mathbf{x}_t, s_{P,t}^k\right) + N(\mathbf{0}, Q_P) \\ &\quad \triangleq v_P'(\mathbf{y}_t, k) + N(\mathbf{0}, Q_P) \end{aligned} \tag{2}$$

where $z_{Pd,t}^j$ and $z_{Pb,t}^j$ are the distance and angle from the robot of the $j$th point measurement, respectively, $c_{P,t}^j \in [1, N]$ is the correspondence variable of $z_{P,t}^j$ and $Q_P$ is the covariance matrix of the point measurement model. If the correspondence variable is less than or equal to $N_G$, a point landmark in the given map is observed. Otherwise, the observed landmark is in the SLAM map. Similarly, the line measurement model is defined in two ways with respect to the map that the observed line belongs to. The line measurement model is formulated as follows:

$$\begin{aligned} &\text{if } \; k = c_{L,t}^j \le M_G \\ &z_{L,t}^j = \begin{bmatrix} z_{Ld,t}^j \\ z_{Lb,t}^j \end{bmatrix} = v_L\left(\mathbf{x}_t, m_P^k\right) + N(\mathbf{0}, Q_L) \\ &\text{else} \\ &z_{L,t}^j = \begin{bmatrix} z_{Ld,t}^j \\ z_{Lb,t}^j \end{bmatrix} = v_L\left(\mathbf{x}_t, s_{L,t}^k\right) + N(\mathbf{0}, Q_L) \\ &\quad \triangleq v_L'(\mathbf{y}_t, k) + N(\mathbf{0}, Q_L) \end{aligned} \tag{3}$$

where $z_{Ld,t}^j$ and $z_{Lb,t}^j$ are the distance and angle from the robot of the $j$th line measurement, respectively, $c_{L,t}^j \in [1, N]$ is the correspondence variable of $z_{L,t}^j$ and $Q_L$ is the covariance matrix of the line measurement model.

Based on those system models and the inputs of $\mathbf{u}_t, \mathbf{z}_t$, and $\mathbf{c}_t$, each hypothesis estimates its own total state vector $\mathbf{y}_t$ by the extended Kalman-filter-based SLAM (EKF-SLAM) algorithm. Then, we will pick the best state vector to make a final decision about the location of the robot.

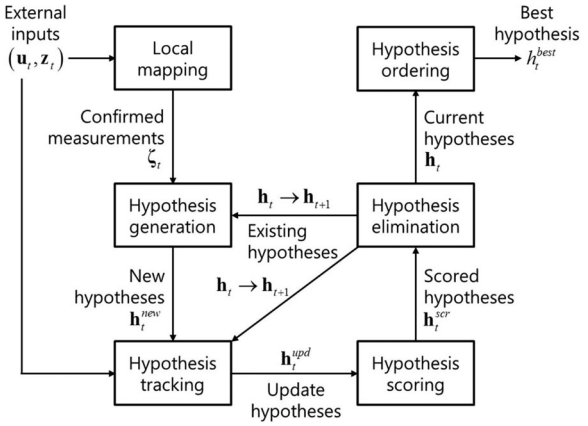


Fig 1. Overview of the SiGLAM algorithm.

## III. SiGLAM Algorithm

Since false alarm measurements have been a problem for feature-driven methods [15]–[18], we tried to analyze and overcome those measurements. False alarms have two sources: 1) temporary noise of sensor measurement and 2) unregistered landmarks that exist in reality but do not belong to the given map. The unregistered landmarks let false alarms occur constantly at the same location. They make the given map imperfect and severely deteriorate the credit of the true hypothesis, which represents the true pose of a robot.

The SiGLAM algorithm presented in this section can deal with this problem using three main ideas. First, once an unregistered landmark is detected, it is inserted into the SLAM map and will never be considered a false alarm again. Second, hypotheses are continuously generated whenever possible because we suspect that the measurements from which initial hypotheses are created can possibly be false alarms. Third, since the second idea does not allow multiple hypotheses to converge, the credibility of each hypothesis must be evaluated in a way that is extremely robust to sensor noise.

Total hypotheses at time $t$ are denoted by $\mathbf{h}_t = \left\{h_t^i\right\}_{i=1}^{D_t}$ when there exist $D_t$ hypotheses. The $i$th hypothesis is represented by $h_t^i = (\ \mu_{\mathbf{y},t}^i \quad \Sigma_{\mathbf{y},t}^i \quad \sigma_t^i\ )$, each represents the mean and covariance of the total state vector $\mathbf{y}_t$ of the hypothesis and the score of the hypothesis, respectively.

In order to estimate and manage the hypotheses $\mathbf{h}_t$, the SiGLAM algorithm is designed as illustrated in Fig. 1. A detailed description of each module is given in the following subsections.

### A. Hypothesis Generation

In an environment that consists of line and point landmarks, the possible robot poses can be specified in the map by matching a pair of line and point measurements with a pair of line and point landmarks [20]. Multiple positions can be specified at once because the relationship between the detected line and point landmarks is normally not unique, due to the repetitive and symmetric properties of an indoor environment.

The local mapping process is used to filter out outlying measurements. We simply determine that a landmark consecutively detected more than $T_C$ times is considered to exist in reality. It preserves only the currently observed landmarks and rejects the others, counting the number of detected times for each landmark. Its output is the subset of measurements observed from certainly existing landmarks, called confirmed measurements, denoted by $\zeta_t = (\ \zeta_{P,t}^{1:\eta_P} \quad \zeta_{L,t}^{1:\eta_L}\ )$, where $\zeta_t \subset \mathbf{z}_t$. Moreover, in order to avoid generating duplicate hypotheses, the hypothesis generation process is triggered only when the confirmed measurements are observed from the new combination of landmarks in the local map, which are different from the landmark set used for the most recent hypothesis generation. When the number of confirmed line measurements or point measurements, $\eta_L$ or $\eta_P$, is larger than one, the extra confirmed measurements are welcomed for further verification of new hypotheses.

The first of the hypothesis generation is data association for confirmed measurements. Earlier works found possible poses by using a tree structure, but we specify the possible poses with the least geometric constraints and then verify them with the extra constraints. The least geometric constraint is the distance between a single pair of line and point landmarks. The confirmed measurement pair $\zeta_{P,t}^1$ and $\zeta_{L,t}^1$ is matched to the landmark pair $m_P^i$ and $m_L^k$ if the distance between the measurement pair is the same as the distance between the landmark pair. Practically, we consider that the measurement pair is matched with the landmark pair when the difference between the distances of the pairs is lower than the threshold $T_D$. All the matched pairs of landmarks are searched on the given map and each of them is used for specifying a possible pose. For instance, for a matched pair of landmarks $m_P^i$ and $m_L^k$, the corresponding pose is computed by

$$\begin{aligned}[\hat{x} \quad \hat{y} \quad \hat{b}]' &= f\left(m_P^i, m_L^k, \zeta_{P,t}^1, \zeta_{L,t}^1\right) \\ &\triangleq \begin{bmatrix} m_{Px}^i - \zeta_{Pd,t}^1 \cos\left(\zeta_{Pb,t}^1 + m_{Lb}^k - \zeta_{Lb,t}^1\right) \\ m_{Py}^i - \zeta_{Pd,t}^1 \sin\left(\zeta_{Pb,t}^1 + m_{Lb}^k - \zeta_{Lb,t}^1\right) \\ m_{Lb}^k - \zeta_{Lb,t}^1 \end{bmatrix}. \end{aligned} \tag{4}$$

This is not an optimal solution but it will be optimized by the EKF update. If the remainder of the confirmed measurements is matched to the given landmarks with respect to the pose obtained by (5) and the pose is not overlapped by any of the existing hypotheses, then the pose is added as a new hypothesis. A new hypothesis is initialized as follows:

$$\begin{aligned} D_t &= D_t + 1 \\ h_t^{D_t} &= \left[\mu_{\mathbf{y},t}^{D_t} \quad \Sigma_{\mathbf{y},t}^{D_t} \quad \sigma_t^{D_t}\right] \\ \mu_{\mathbf{y},t}^{D_t} &= [x_t' \ \ y_t' \ \ b_t'], \quad \Sigma_{\mathbf{y},t}^{D_t} = F^T \begin{bmatrix} Q_P & \mathbf{0} \\ \mathbf{0} & Q_L \end{bmatrix} F, \quad \sigma_t^{D_t} = 1 \\ F &= \frac{\partial f\left(m_P^i, m_L^k, \zeta_{P,t}^1, \zeta_{L,t}^1\right)}{\partial \left[\zeta_{P,t}^{1\,T} \quad \zeta_{L,t}^{1\,T}\right]^T} \end{aligned} \tag{5}$$

where $Q_P$ and $Q_L$ are defined in Section II. The result of the hypotheses generation is depicted in Fig. 2. We can see that

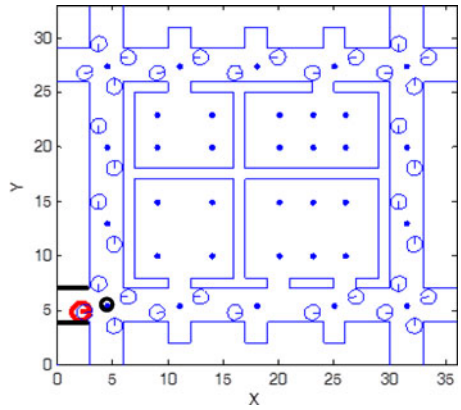


Fig. 2. Initially generated hypotheses. Line and point landmarks are denoted by thin lines and points, respectively. The thick directed circle on the lower left represents the true pose of a robot. The thick lines and circle denote the confirmed line and point measurements, respectively. The initially generated hypotheses are marked as thin directed circles on similar patterns of landmarks.

there is one hypothesis overlapped with the true pose. Now we have to track the hypotheses and find the true one.

### B. Hypothesis Tracking

In order to evaluate the credibility of hypotheses from their history, we have to keep track of the hypotheses. In addition, if a hypothesis observes an unregistered landmark, it is incorporated into the SLAM map and estimated by the EKF-SLAM algorithm. The posterior representation of the total state vector of the $i$th hypothesis $\mathbf{y}_t^i$ is expanded as follows:

$$\begin{aligned}
bel(\mathbf{y}_t^i) &= p(\mathbf{y}_t^i|\mathbf{m},\mathbf{u}_{1:t},\mathbf{z}_{1:t},\mathbf{c}_{1:t}) \\
&= \eta p(\mathbf{z}_t|\mathbf{y}_t^i,\mathbf{m},\mathbf{u}_{1:t},\mathbf{z}_{1:t-1},\mathbf{c}_{1:t}) \\
&\quad \times p(\mathbf{y}_t^i|\mathbf{m},\mathbf{u}_{1:t},\mathbf{z}_{1:t-1},\mathbf{c}_{1:t}) \\
&= \eta p(\mathbf{z}_t|\mathbf{y}_t^i,\mathbf{m},\mathbf{c}_t) \\
&\quad \int p(\mathbf{y}_t^i|\mathbf{y}_{t-1}^i,\mathbf{m},\mathbf{u}_{1:t},\mathbf{z}_{1:t-1},\mathbf{c}_{1:t}) \\
&\quad \times p(\mathbf{y}_{t-1}^i|\mathbf{m},\mathbf{u}_{1:t},\mathbf{z}_{1:t-1},\mathbf{c}_{1:t}) d\mathbf{y}_{t-1}^i \\
&= \eta p(\mathbf{z}_t|\mathbf{y}_t^i,\mathbf{m},\mathbf{c}_t) \int p(\mathbf{y}_t^i|\mathbf{y}_{t-1}^i,\mathbf{m},\mathbf{u}_{1:t},\mathbf{z}_{1:t-1},\mathbf{c}_{1:t}) \\
&\quad \times bel(\mathbf{y}_{t-1}^i) d\mathbf{y}_{t-1}^i \\
&= \eta p(\mathbf{z}_t|\mathbf{y}_t^i,\mathbf{m},\mathbf{c}_t) \times \overline{bel}(\mathbf{y}_t^i) \\
&= \eta \overline{bel}(\mathbf{y}_t^i) \times \prod_{j=1}^{n_P} p(z_{P,t}^j|\mathbf{x}_t,\mathbf{s}_t,\mathbf{m},\mathbf{c}_t) \\
&\quad \times \prod_{j=1}^{n_L} p(z_{L,t}^j|\mathbf{x}_t,\mathbf{s}_t,\mathbf{m},\mathbf{c}_t) \\
&= \eta \overline{bel}(\mathbf{y}_t^i) \times \prod_{\substack{j=1 \\ c_{P,t}^j \le N_G}}^{n_P} p(z_{P,t}^j|\mathbf{x}_t,\mathbf{m},\mathbf{c}_t) \\
&\quad \times \prod_{\substack{j=1 \\ c_{L,t}^j \le M_G}}^{n_L} p(z_{L,t}^j|\mathbf{x}_t,\mathbf{m},\mathbf{c}_t) \\
&\quad \times \prod_{\substack{j=1 \\ c_{P,t}^j > N_G}}^{n_P} p(z_{P,t}^j|\mathbf{x}_t,\mathbf{s}_t,\mathbf{c}_t) \\
&\quad \times \prod_{\substack{j=1 \\ c_{L,t}^j > M_G}}^{n_L} p(z_{L,t}^j|\mathbf{x}_t,\mathbf{s}_t,\mathbf{c}_t). \qquad (6)
\end{aligned}$$

The posterior is proportional to the product of the five terms in the last line in (8). The first term $\overline{bel}(\mathbf{y}_t^i)$ is the state distribution predicted by the motion information of a robot. The prediction step follows the basic EKF equations that result in the predicted parameters $\bar{\mu}_{\mathbf{y},t}$ and $\bar{\Sigma}_{\mathbf{y},t}$.

The next two terms represents state correction by using measurements corresponding to the given landmarks. For point measurements of which $k = c_{P,t}^j \le N_G$, the Kalman gain is computed as follows:

$$\begin{aligned}
V_{P,t}^k &= \frac{\partial v_P\left(\mu_{\mathbf{x},t}, m_P^k\right)}{\partial \mu_{\mathbf{y},t}} \\
K_{P,t}^k &= \bar{\Sigma}_{\mathbf{y},t} V_{P,t}^{kT} \left(V_{P,t}^k \bar{\Sigma}_{\mathbf{y},t} V_{P,t}^{kT} + Q_P\right)^{-1} \qquad (7)
\end{aligned}$$

where $\bar{\mu}_{\mathbf{x},t}$ and $\bar{\Sigma}_{\mathbf{x},t}$ are parts of $\bar{\mu}_{\mathbf{y},t}$ and $\bar{\Sigma}_{\mathbf{y},t}$, respectively, corresponding to the robot's pose. Similarly, for line measurement of which correspondence variable is $k = c_{P,t}^j \le N_G$, the Kalman gain is obtained by

$$\begin{aligned}
V_{L,t} &= \frac{\partial v_L\left(\mu_{\mathbf{x},t}, m_L^k\right)}{\partial \mu_{\mathbf{y},t}} \\
K_{L,t}^k &= \bar{\Sigma}_{\mathbf{y},t} V_{L,t}^{kT} \left(V_{L,t}^k \bar{\Sigma}_{\mathbf{y},t} V_{L,t}^{kT} + Q_L\right)^{-1}. \qquad (8)
\end{aligned}$$

The last two terms in (6) are almost the same as the correction step of SLAM, in that they update the total state using measurements corresponding to the SLAM landmarks. The EKF update equations for point measurements of $k = c_{P,t}^j > N_G$ and line measurements of $k = c_{L,t}^j > M_G$ are the same as (7) and (8), but only the Jacobians are calculated differently as follows:

$$V_{P,t}^k = \frac{\partial v_P'\left(\mu_{\mathbf{y},t}, k\right)}{\partial \mu_{\mathbf{y},t}} \qquad (9)$$

$$V_{L,t}^k = \frac{\partial v_L'\left(\mu_{\mathbf{y},t}, k\right)}{\partial \mu_{\mathbf{y},t}}. \qquad (10)$$

With the aforementioned equations, the posterior of the state of each hypothesis is estimated in the EKF framework. The correspondence variables $\mathbf{c}_t$ are assumed to be given where data association, in fact, is solved by the maximum likelihood method [21].

Fig. 3 shows the result of SLAM of the true hypothesis. The original map is depicted in the left-side image, while the right-side image additionally shows the SLAM landmarks of the true hypothesis. The unregistered landmarks detected by a robot become the SLAM landmarks. After the robot traveled

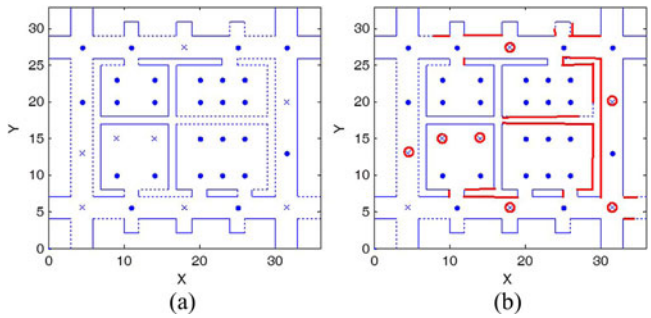


Fig. 3. (a) Original map. (b) The SLAM map is overlapped on the original map. The given line and point landmarks are denoted by solid lines and points and the unregistered line and point landmarks are denoted by dotted lines and x-marks. Thick lines and circles are SLAM landmarks.

around the environment once, the hypothesis will recognize 21 more line landmarks and 7 more point landmarks, aside from the given landmarks.

### C. Hypothesis Scoring

Since we retain multiple hypotheses that have not converged to one, hypothesis scoring is the most important part of the algorithm. As mentioned before, the likelihood of a hypothesis is not a reliable measure of hypothesis credibility. Rather, the hypothesis score is computed from data association records over the whole history of the hypothesis. In this paper, the hypothesis score is evaluated by the number of supportive landmarks minus the number of unsupportive landmarks. The supportive landmarks refer to the given landmarks observed by the hypothesis, and the unsupportive landmarks are the SLAM landmarks estimated by the hypothesis. Thus the score of the $i$th hypothesis is calculated as follows:

$$\sigma_t^i = \left(\widehat{N}_{G,t}^i + \widehat{M}_{G,t}^i\right) - \left(N_{S,t}^i + M_{S,t}^i\right) \tag{11}$$

where $\widehat{N}_{G,t}^i$ and $\widehat{M}_{G,t}^i$ are the number of point and line supportive landmarks detected by the hypothesis until time $t$, respectively, and $\widehat{N}_{S,t}^i$ and $\widehat{M}_{S,t}^i$ are the number of point and line unsupportive landmarks at time $t$, respectively. This scoring policy depends on the trajectory of the robot and a structure of the environment and is immune to sensor noise. If a robot experiences a sufficiently large area that is unique in the map, then the single best hypothesis will arise above the others.

### D. Hypothesis Elimination

The SiGLAM algorithm preserves the true hypothesis from measurement errors and an imperfect map. Theoretically, hypothesis elimination is not an essential part of this algorithm. However, as new hypotheses are continuously added from the hypothesis generation section, some false hypotheses should be removed to prevent the computational load from increasing constantly. We eliminate only clearly false hypotheses that satisfy one of the three conditions: 1) hypothesis score below 0; 2) hypothesis passing through a wall; and 3) hypothesis beyond the margins of the given map. The first condition means that there is more negative evidence than supportive evidence on a false hypothesis. The second condition is a physical constraint. If a hypothesis passes though a line landmark and then fails on data association for a certain period of time, the hypothesis is considered to have passed through a wall. The third condition is an assumption of the SiGLAM problem that a robot must be found in the target environment.

After elimination, the current hypotheses in Fig. 1 are ordered with respect to their scores, and then we can see that is most scored. The most scored hypothesis is assured to be the best hypothesis, $h_t^{\text{best}}$, when the score difference is larger than the minimum score difference, $T_S$. This is the end of the algorithm description. The proposed method tracks all the possibilities for global localization of a robot. Compared to the existing feature-driven methods, our method is more conservative and reliable and is not so dependent on parameters. This method is demonstrated in the simulations and experiments in the next sections.

## IV. Simulation Results

Simulations were conducted for performance verification of the proposed algorithm. The proposed algorithm is compared with the Monte Carlo localization (MCL) [22] and the contemporary feature-driven methods [18] that are briefly introduced in Section IV-B. The algorithms were tested with different maps and parameters through different trajectories to evaluate their performance in various situations. We designed the three maps shown in Fig. 4 such that each has distinctive properties that represent various aspects of the real world. The first map (M1) is static and symmetric, the second map (M2) is static and unsymmetrical, and the third map (M3) is dynamic and symmetric. Detailed descriptions of the maps are given in the later subsections.

In order to implement the imperfection of the map, a new parameter, hidden map ratio $R_H$, is introduced. If the hidden map ratio is 0.1, one in ten landmarks is randomly selected and "hidden". In other words, a robot can detect all the landmarks to obtain measurements but the hidden landmarks are not supplied to the localization algorithms and are the unregistered landmarks defined in Section III. The hidden map ratio is varied by 0.1 from 0.0 to 0.3.

For the statistical reliability of the simulation results, a robot traveled through 20 different trajectories for the same period of time in each map, recording odometry and measurement inputs. Therefore, the algorithms were tested through twenty trajectories in each of the three maps with each of the four hidden map ratios for a total of 240 times. The simulation results from twenty trajectories in the same situation were averaged and the performance table was finally presented for the twelve different situations. The results from the three maps are presented in Sections IV-C–IV-E, respectively.

The performance of the algorithms is evaluated using four measures. The first is the correct localization rate (CLR), which is the ratio of the number of time steps that a robot successfully localizes over the total number of time steps. As the CLR approaches 100%, the algorithm works perfectly over the whole simulation time. The second is the false localization rate (FLR),

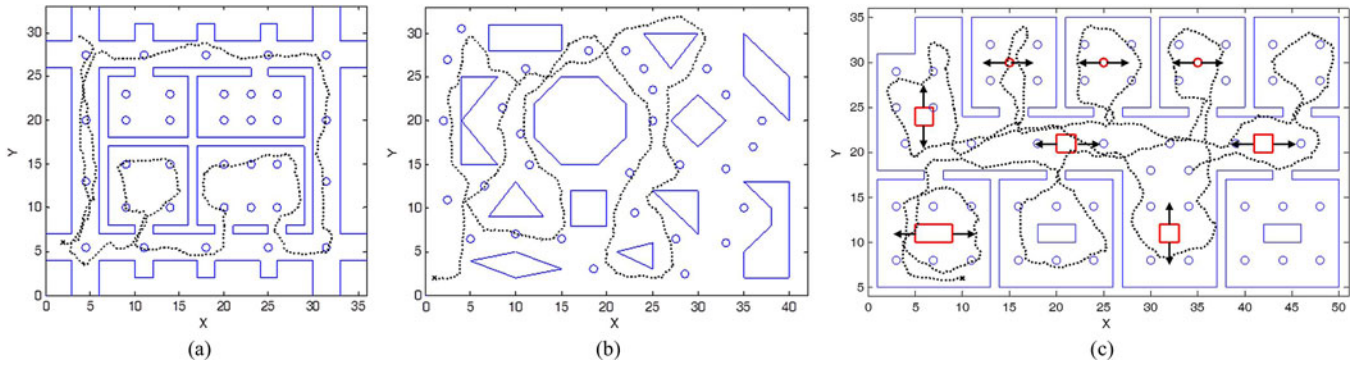


Fig. 4. Simulation environments. (a) Static and symmetric map M1. (b) Static and unsymmetric map M2. (c) Dynamic and symmetric map M3. The trajectories represent the first trajectories in each map and the x marks denote the starting points.

which is the ratio of the number of time steps that a robot has localized at a wrong location over the total number of time steps. False localization is dangerous because it can lead to a wrong decision during motion planning. The third measure is the localization failure rate (LFR), which is the percentage of time that the algorithm fails to localize a robot. CLR, FLR and LFR must sum to 100%. The last measure is the first correct localization time (FCLT), which is computed by averaging the time steps when a robot is first localized at the correct location. The FCLT measures how quickly an algorithm finds the true pose. The four measures are described in order of importance. CLR shows a primal localization performance and FLR represents reliability of localization result while the others give additional properties.

Once the true pose is detected, every algorithm can keep track of the true trajectory in a perfect map. We are not interested in an accuracy of the pose estimation but whether a localization algorithm is tracking the true position or not. This is because the local localization performance depends on parametric tuning rather than on a tracking method. We admit that global localization is achieved when the position difference between the estimated position and the ground truth position is within the threshold.

### A. Parameters

When implementing the simulation environment, several noise parameters are required for input acquisition. The motion and measurement models are corrupted by Gaussian noise with a zero mean as defined in (1)–(3). The covariance matrix of motion noise is set to $R = \mathrm{diag}\,(\,0.01 \quad 0.01 \quad 0.001\,)$, and the covariance matrices of both line and point measurement are set to $Q_L = Q_P = \mathrm{diag}\,(\,0.01 \quad 0.001\,)$. In all of the simulations, the same noise covariance matrices are applied.

In the SiGLAM algorithm description, several parameters were introduced and they are tuned empirically through simulations. For local mapping, $T_C$ is selected to be 3 so that confirmed measurements are not obtained from noisy measurements but obtained as frequently as possible. In hypothesis generation, $T_D$ is set to 0.5, which is five times the standard deviation of the distance measurement noise. The value of $T_D$ is shared with the other methods defined in the subsequent section for data association of features. At the tail of the SiGLAM algorithm, the best hypothesis is selected when the most scored hypothesis gets a higher score than the second-most scored hypothesis by the minimum score difference $T_S$. Since $T_S$ directly affects the localization output, it should be carefully selected. Simulations were carried out with different values of $T_S$, 1–5, in order to see the effect of this parameter while the hidden map ratio is fixed at 0.2. The results are summarized in Table II, which clearly shows that both CLR and FLR decrease as $T_S$ increases, regardless of the maps. In addition, we can see that lower $T_S$ values result in lower FCLT measures, which means hasty localization. Overall, there is a tradeoff between reliability and promptness. Therefore, we selected the intermediate value 3 for $T_S$ to obtain relatively high performance while keeping the risk low.

TABLE II
SIMULATION RESULTS OF SIGLAM WITH DIFFERENT $T_s$ VALUES

| Map | $T_s$ | CLR (%) | FLR (%) | LFR (%) | FCLT |
|---|---|---|---|---|---|
| M1 | 1 | 81.67 | 9.83 | 8.50 | 79.2 |
| | 2 | 79.99 | 5.38 | 14.63 | 89.0 |
| | 3 | 78.06 | 2.99 | 18.95 | 102.7 |
| | 4 | 75.18 | 2.43 | 22.39 | 114.5 |
| | 5 | 72.79 | 1.69 | 25.52 | 132.8 |
| M2 | 1 | 92.52 | 2.81 | 4.67 | 26.6 |
| | 2 | 91.95 | 2.10 | 5.95 | 28.5 |
| | 3 | 91.24 | 1.65 | 7.11 | 29.7 |
| | 4 | 90.56 | 1.32 | 8.12 | 30.7 |
| | 5 | 89.41 | 1.02 | 9.57 | 33.4 |
| M3 | 1 | 75.89 | 13.16 | 10.95 | 83.9 |
| | 2 | 72.57 | 8.35 | 19.08 | 99.1 |
| | 3 | 68.63 | 5.21 | 26.16 | 110.8 |
| | 4 | 66.34 | 3.52 | 30.14 | 127.5 |
| | 5 | 62.89 | 2.25 | 34.86 | 136.2 |

### B. Comparative Methods

The proposed method is compared with four other algorithms by feeding all the five algorithms the same inputs from the simulations. Two of the other algorithms are MCL with 500 and 3000 particles, which are denoted by *MCL500* and *MCL3000*, respectively. The initial particles are randomly distributed over a map and are managed by the particle filter algorithm. If the variance in particle pose is below the threshold, it is considered to be converged and so localized and then the mean pose of

the particles is returned as a localization output. After localization, the particles are reinitialized if the overall data association results of the converged particles are consecutively poor.

The two other algorithms are the feature-driven methods proposed by Kar [18]. Since this method can be interpreted in two ways, we implemented both. The difference between the methods depends upon making a decision on localization. Localization is achieved when a single hypothesis survives but also when there exists the hypothesis with the largest likelihood among the most paired hypotheses. FDM_single denotes the former algorithm and FDM_best the latter. The two algorithms generate, track and eliminate hypotheses in the same manner but select the best hypothesis differently. Since the type of landmark in this paper is different from [18], hypothesis generation, tracking, and data association methods are adopted from our method while hypothesis rejection methods follow the original work. A hypothesis is rejected when the ratio of the associated features over the detected features is lower than the data overlap threshold $\eta$, or when hypotheses are duplicated at the same place. The comparisons between the proposed method and the four comparative methods in the three maps are presented in the following subsections.

TABLE III
PERFORMANCE TABLE RESULTING FROM M1

| $R_H$ | Method | CLR (%) | FLR (%) | LFR (%) | FCLT |
|---|---|---|---|---|---|
| 0.3 | MCL500 | 4.27 | 76.99 | 18.74 | 121.0 |
| | MCL3000 | 12.53 | 75.16 | 12.31 | 115.0 |
| | FDM_best | 35.67 | 57.69 | 6.64 | 57.4 |
| | FDM_single | 29.42 | 21.37 | 49.21 | 85.2 |
| | SiGLAM | 79.44 | 2.28 | 18.28 | 87.2 |
| 0.2 | MCL500 | 6.11 | 79.30 | 14.59 | 178.3 |
| | MCL3000 | 13.25 | 75.32 | 11.43 | 43.2 |
| | FDM_best | 48.17 | 48.87 | 2.96 | 59.7 |
| | FDM_single | 40.62 | 17.64 | 41.74 | 109.7 |
| | SiGLAM | 76.65 | 5.99 | 17.36 | 99.3 |
| 0.1 | MCL500 | 18.23 | 71.69 | 10.08 | 107.7 |
| | MCL3000 | 31.05 | 61.02 | 7.93 | 206.3 |
| | FDM_best | 70.80 | 27.81 | 1.39 | 44.1 |
| | FDM_single | 63.06 | 8.82 | 28.12 | 98.9 |
| | SiGLAM | 82.33 | 4.08 | 13.59 | 86.0 |
| 0.0 | MCL500 | 28.15 | 63.61 | 8.24 | 133.1 |
| | MCL3000 | 45.14 | 49.99 | 4.87 | 146.2 |
| | FDM_best | 91.98 | 7.68 | 0.34 | 12.8 |
| | FDM_single | 84.22 | 0.62 | 15.16 | 79.8 |
| | SiGLAM | 87.34 | 0.00 | 12.66 | 64.0 |

### C. Symmetric Environment

The map shown in Fig. 4(a) is denoted by M1 and is relatively small, static and symmetric. M1 consists of 84 line landmarks and 34 point landmarks. Small and static properties are favorable to global localization but the symmetric property results in ambiguous localization. The symmetric property implies that similar patterns are repeated over a map. In this map, a robot traveled 20 times for the same period of time, 500 time steps. This simulation is designed to see how quickly each method overcomes the ambiguity of the symmetric map conditioned on different values of the hidden map ratio.

The performance of each of the five methods is presented in Table III. The table notes that the overall performances are arranged as *MCL500*, *MCL3000*, FDM_single, FDM_best, and SiGLAM in ascending order. Hiding more landmarks deteriorates the whole performance and it crucially affects the feature-driven methods. The CLR of FDM_single drops from 91.98% to 36.67% and that of FDM_best drops from 84.22% to 29.42% as $R_H$ increases. This is because the feature-driven methods are re-initialized when the ratio of unexpected features is over the threshold. On the contrary, SiGLAM works effectively even in the difficult cases because SiGLAM does not eliminate hypotheses based on the current observations but on the historical score of a hypothesis. The MCL algorithms, on the other hand, generally perform poorly. It seems excessively risky from that the CLR and LFR are low and FLR is high. The MCL algorithms are not reliable even in the perfect map ($R_H = 0$) because the symmetric property of M1 may let particles converge at wrong locations. With the perfect map, FDM_best outperforms SiGLAM in terms of CLR because FDM_best can quickly achieve localization right after initial hypotheses are generated. This is assured by the extremely low LFR and FCLT of FDM_best at $R_H = 0$. Alternatively, SiGLAM must wait to return the localization output until the score difference diverges. However, it should be noted that SiGLAM almost never makes false localization at $R_H = 0$ and is very unlikely to make false localization even at $R_H > 0$.

### D. Unsymmetric Environment

The second map shown in Fig. 4(b) is static and unsymmetric. It consists of 52 line landmarks and 30 point landmarks. Since all of the properties are advantageous for global localization, the overall performances are expected to be high. A robot traveled 600 time steps in each simulation in this map.

The simulation results are summarized in Table IV. The overall performance is similar to Table III but slightly higher. SiGLAM maintains high performance in spite of the existence of unregistered landmarks while the performances of the others vary greatly with $R_H$. It is different from M1 that the localization accuracy of the MCL algorithms greatly improves at low $R_H$ values. Instant observation of features can lead to unambiguous global localization because the pattern of landmarks in M2 is seldom repeated. The MCLs work effectively in the unsymmetric perfect map but not efficiently. The process time is relatively large, 35 ms for *MCL500* and 223 ms for *MCL3000* on average, compared with 1 ms for SiGLAM.

The feature-driven methods tend to achieve first correct localizations more quickly due to their prompt hypothesis elimination strategy, while SiGLAM manages hypotheses in a more conservative manner. The proposed method and the feature-driven methods show similarly high performance at $R_H$ close to zero but the difference between them diverges as $R_H$ increases.

TABLE IV
PERFORMANCE TABLE RESULTING FROM M2

| $R_H$ | Method | CLR (%) | FLR (%) | LFR (%) | FCLT |
|---|---|---|---|---|---|
| | MCL500 | 23.18 | 50.48 | 26.35 | 159.0 |
| | MCL3000 | 36.09 | 41.49 | 22.42 | 133.3 |
| 0.3 | FDM_best | 44.79 | 19.21 | 36.00 | 36.7 |
| | FDM_single | 42.79 | 14.28 | 42.93 | 37.6 |
| | SiGLAM | 82.01 | 4.01 | 13.98 | 52.8 |
| | MCL500 | 26.46 | 48.97 | 24.58 | 176.0 |
| | MCL3000 | 50.83 | 32.53 | 16.63 | 73.3 |
| 0.2 | FDM_best | 64.32 | 14.94 | 20.74 | 17.3 |
| | FDM_single | 60.89 | 11.11 | 28.00 | 20.2 |
| | SiGLAM | 87.48 | 2.93 | 9.58 | 24.1 |
| | MCL500 | 53.75 | 33.58 | 12.67 | 121.1 |
| | MCL3000 | 71.67 | 18.96 | 9.38 | 82.7 |
| 0.1 | FDM_best | 85.32 | 7.05 | 7.63 | 21.1 |
| | FDM_single | 83.02 | 4.45 | 12.53 | 24.2 |
| | SiGLAM | 93.08 | 0.81 | 6.11 | 24.5 |
| | MCL500 | 67.26 | 23.94 | 8.80 | 190.3 |
| | MCL3000 | 84.67 | 10.78 | 4.56 | 73.3 |
| 0.0 | FDM_best | 98.10 | 0.14 | 1.76 | 4.6 |
| | FDM_single | 96.21 | 0.00 | 3.79 | 9.6 |
| | SiGLAM | 96.46 | 0.01 | 3.53 | 15.3 |

TABLE V
PERFORMANCE TABLE RESULTING FROM M3

| $R_H$ | Method | CLR (%) | FLR (%) | LFR (%) | FCLT |
|---|---|---|---|---|---|
| | MCL500 | 8.66 | 67.11 | 24.24 | 259.7 |
| | MCL3000 | 9.88 | 69.36 | 20.76 | 336.2 |
| 0.3 | FDM_best | 18.80 | 50.36 | 30.85 | 106.8 |
| | FDM_single | 15.79 | 29.56 | 54.66 | 145.2 |
| | SiGLAM | 66.65 | 6.28 | 27.08 | 164.0 |
| | MCL500 | 9.25 | 70.70 | 20.06 | 331.4 |
| | MCL3000 | 16.58 | 65.62 | 17.80 | 240.5 |
| 0.2 | FDM_best | 31.86 | 49.84 | 18.30 | 62.6 |
| | FDM_single | 26.49 | 26.23 | 47.28 | 135.5 |
| | SiGLAM | 82.89 | 3.82 | 13.30 | 138.6 |
| | MCL500 | 21.54 | 63.20 | 15.27 | 205.0 |
| | MCL3000 | 30.24 | 58.10 | 11.67 | 317.9 |
| 0.1 | FDM_best | 54.26 | 35.83 | 9.92 | 36.2 |
| | FDM_single | 46.13 | 14.39 | 39.49 | 71.2 |
| | SiGLAM | 87.12 | 2.48 | 10.41 | 105.6 |
| | MCL500 | 21.58 | 65.42 | 13.01 | 426.5 |
| | MCL3000 | 68.63 | 27.56 | 3.81 | 259.4 |
| 0.0 | FDM_best | 83.21 | 13.71 | 3.09 | 26.1 |
| | FDM_single | 77.24 | 2.08 | 20.68 | 67.5 |
| | SiGLAM | 90.95 | 0.26 | 8.79 | 82.3 |

### *E. Dynamic Environment*

The last map, denoted by M3, is dynamic and symmetric at a relatively large scale. It consists of 76 line landmarks and 51 point landmarks. In addition, there are 20 dynamic line landmarks and three dynamic point landmarks that are, of course, not involved in the given map. In contrast to M2, M3 is a challenging environment for global localization. A robot traveled for 1000 time steps for each simulation. This map is designed to test the ability of the algorithms that can overcome dynamic objects. The dynamic objects are implemented as moving rectangles and moving points that are, respectively, denoted by red thick lines and circles in Fig. 4(c). They move horizontally or vertically in the restricted ranges by a random walk with uniform noise$U(-0.5, 0.5)$.

The simulation results are given in Table V. As expected, the overall performances are degraded in that CLRs are decreased and FLR, LFR, and FCLT are increased, compared with M1 and M2. In the case of $R_H = 0.3$, the combination of hidden landmarks and dynamic objects significantly deteriorates the localization performance of the four comparative methods while SiGLAM is relatively less affected. The MCLs and feature-driven methods seem not to work reliably except for the case of the perfect map. Overall, FLCTs increased more than three times compared with that of M2. This means that dynamic (hidden) objects interfere with the true hypothesis to acquire relatively high credibility. Interestingly, SiGLAM outperforms all other algorithms in the perfect M3 due to dynamic objects, considering that FDM_best showed a better performance in the perfect M1 and M2. In addition, SiGLAM maintains low FLR, from 0.26% to 6.28%, in spite of hidden landmarks and dynamic objects.

So far, we have analyzed the simulation results from the three maps with the four different hidden map ratios. The results support the theory that the proposed method generally shows high localization accuracy and its overwhelming capability is exhibited especially in the challenging environment. The best aspect of SiGLAM is its low FLR, which allows localization results to be trusted.

## V. EXPERIMENTAL RESULTS

Since the proposed algorithm is motivated by trouble in practical applications, SiGLAM and the other methods were tested in real world experiments where ceiling edges and electric lamps are detected and used as natural line and point landmarks, respectively.

The experiment data was obtained from two places. The first dataset was acquired on the fourth floor of the Korea Electronics Technology Institute (KETI) and is denoted by *KETI_4 F*. The second dataset was obtained on the seventh floor of Engineering Building three at Yonsei University and is simply denoted by *EB_7 F*.

In the both experiments, the robot's velocity was recorded and the ceiling image was collected at each sampling time. Ceiling images were captured by a mono camera looking up the ceiling that is mounted on the top of the robot. We used the two mobile robots shown in Fig. 5. A Dasa mobile platform equipped with the embedded camera is shown in Fig. 5(a) and is used for the KETI experimentation. The embedded camera outputs 320 $\times$ 240 gray scale images. For experimentation in the Engineering Building, the Pioneer 3-DX shown in Fig. 5(b) is utilized and is equipped with the Bumblebee2 camera. This camera captures 640 $\times$ 480 stereo colored images but we only used the right-side

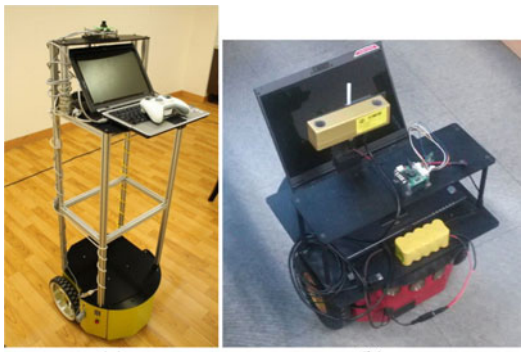

Fig. 5. Mobile robots used for experiments in (a) *KETI_4 F* and (b) *EB_7 F*.

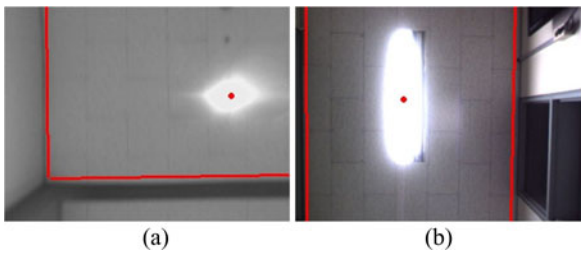

Fig. 6. Feature extraction results from (a) *KETI_4 F* and (b) *EB_7 F*.

images converted to 320 × 240 gray scale images for fast image processing.

From the collected ceiling images, line and point features are extracted. The feature extractor detects line features at the ceiling boundaries as well as point features from electric lamps in the ceiling images. Fig. 6 shows the result of the feature extraction. The extracted features are drawn with red lines and points. A detailed description of the feature extraction method is provided in our previous research [19], [23].

The ground truth trajectory of the robot is estimated by MCL with the known initial pose that is local localization in the given map. The parameters of SiGLAM are the same as in the simulations except that the distance difference threshold is changed to $T_D = 50$ cm. In addition, since the performances of the MCL algorithms depend on random sampling, the localization results vary every time the algorithm is committed. Therefore, we tried the MCL algorithms 20 times with the same dataset and the results were averaged for more reliable performance evaluation.

### A. *KETI_4 F Dataset*

The map of the fourth floor of KETI is depicted in Fig. 7(a) where there are 12 line landmarks and 32 point landmarks. The map is constructed based on the floor plan and verified by hand. The map area is 17.6 × 17.5 $m^2$. The lines stretch long and the points are almost regularly distributed in a line, which contributes to ambiguity during localization. The trajectory in Fig. 7(a) starts from the x mark and travels around the environment more than once. Through the experiment, 5232 ceiling images were collected.

The performance table resulting from the *KETI_4 F* dataset is presented in Table VI. The four comparative methods show rel-

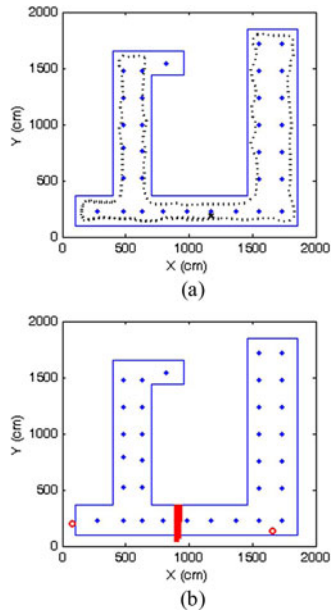


Fig. 7. The map of the fourth floor of Korea Electronics Technology Institute. (a) The original map and the trajectory of the robot. (b) The map completed by SiGLAM. The SLAM map is denoted by thick lines and circles.

TABLE VI
PERFORMANCE TABLE RESULTING FROM *KETI_4 F*

| Method | CLR (%) | FLR (%) | LFR (%) | FCLT |
|---|---|---|---|---|
| MCL500 | 2.16 | 89.01 | 8.83 | 934 |
| MCL3000 | 7.59 | 72.70 | 19.70 | 1056 |
| FDM_best | 32.86 | 33.16 | 33.98 | 96 |
| FDM_single | 27.31 | 0.00 | 72.69 | 481 |
| SiGLAM | 70.37 | 0.00 | 29.63 | 760 |

atively poor performance, although there are a few unregistered landmarks in this environment. Instead, temporarily outlying measurements sometimes occur due to failures in image processing and hinder the true hypothesis from being recognized. In SiGLAM, the true hypothesis was generated during the first hypothesis generation and is never rejected, which results in zero FLR. FDM_single also shows zero FLR and low CLR because FDM_single is a relatively prudent method but easily rejects the true hypothesis due to measurement outliers. So this method is reliable when the map is almost perfect. The localization results of the MCL methods are hard to rely on because of the extremely high FLR.

Fig. 7(b) depicts the SLAM map of the best hypothesis of the SiGLAM algorithm as red thick lines and circles overlaid on the given map after finishing the test. Temporarily outlying measurements are rejected and only the consistently detected measurements are accepted by the SLAM algorithm.

Fig. 8 shows examples of unregistered landmarks in this environment that consists of the SLAM map in Fig 7(b). We expected that only ceiling boundaries are detected by the line feature extractor but the doorframe is also detected due to its strong edge in an image. Moreover, there are more electric lamps than expected. Those unregistered landmarks are registered to the SLAM map and the total map of the environment is completed.

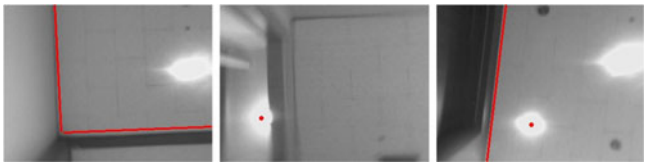

Fig. 8. Unregistered landmarks: a doorframe on the corridor (left), an electric lamp out of the map bound (middle), and an unexpected electric lamp (right).

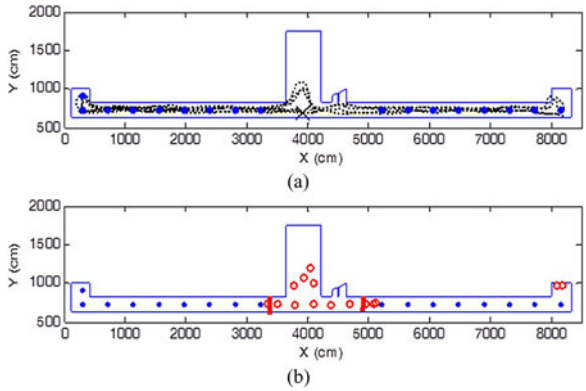


Fig. 9. Map of the seventh floor of the third Engineering Building. (a) The original map and the trajectory of the robot. (b) The map completed by SiGLAM. The SLAM map is denoted by thick lines and circles.

TABLE VII
PERFORMANCE TABLE RESULTING FROM *EB_7 F*

| Method | CLR (%) | FLR (%) | LFR (%) | FCLT |
|---|---|---|---|---|
| MCL500 | 2.18 | 86.94 | 10.88 | 2463 |
| MCL3000 | 5.92 | 73.73 | 20.35 | 1993 |
| FDM_best | 12.85 | 63.56 | 23.60 | 141 |
| FDM_single | 8.42 | 0.70 | 90.88 | 562 |
| SiGLAM | 78.00 | 12.90 | 9.11 | 532 |

### *B. EB_7 F Dataset*

The map of the seventh floor of the Engineering Building is shown in Fig. 9(a). The dotted line represents the ground truth trajectory of the robot that started from the x-mark. The robot traveled around the long corridor about two and half times and took 5823 samples. The map is comprised of 20 line landmarks and 17 point landmarks. The point landmarks represent the long electric lamps while the small lamps are unregistered. The map area is $12 \times 82$ m$^2$ and is horizontally wide, vertically narrow and extremely symmetric.

The performance table resulting from the *EB_7 F* dataset is given in Table VII. The performance difference between SiGLAM and the others now diverges more. The CLRs of the feature-driven methods are degraded to about one-third of those of *KETI_4 F*. This is because of increased symmetry of the map and unregistered landmarks. However, in spite of these conditions, the performances of SiGLAM improved because the robot traveled more than twice in the environment. After fully exploring the environment, SiGLAM can create a complete map of the environment. Once the map is completed, there is no chance for the score of the true hypothesis to be changed or for the other hypotheses to obtain a top score. The false localizations of SiGLAM happened only before one round trip.

Fig. 10. Unregistered landmarks: small lamps (left), a doorframe (middle), and an exit lamp (right).

Fig. 9(b) shows the map completed by SiGLAM where the SLAM landmarks are denoted by red thick lines and circles. The true hypothesis has detected two more line landmarks and 15 more point landmarks. In the middle of the map, small lamps are gathered where the four comparative methods that are successfully tracking the true pose turned to failure. Unregistered landmarks enrolled in the SLAM map are shown in Fig. 10. Small lamps are not included in the given map and line landmarks at the doorframes and a point landmark from the exit lamp are unexpected from the floor plan.

## VI. CONCLUSION

We formulated a new localization problem called SiGLAM, which has existed and proposed a solution to it. The problem involves global localization in an imperfect map and the solution requires combining the feature-driven method and the SLAM algorithm. This work is motivated by practical situations in which false alarm measurements hinder the true pose to be detected. The SiGLAM algorithm is designed to save the true hypothesis from false alarms and to bestow the highest score on the true hypothesis. The proposed method generates, tracks, and scores hypotheses while each hypothesis builds a map of unregistered landmarks. After building a complete map, the score of the true hypothesis is maintained until the environment changes.

The simulations and experiments suggest that SiGLAM generally outperforms existing methods, especially in difficult situations. In the simulations, we tested the effect of unregistered landmarks on global localization performance of each algorithm in the three maps with different characteristics. The SiGLAM algorithm is proven to be least affected by unregistered landmarks. In experiments, the algorithms suffer from temporarily outlying measurements. The true hypothesis of the feature-driven methods and the true particles of MCLs are eliminated by outlying measurements while SiGLAM does not use those measurements for hypothesis scoring. Therefore, we conclude that SiGLAM performs outstandingly in terms of a high CLR and low FLR.

However, there are situations in which SiGLAM does not work. If there are unregistered landmarks that are more frequent than given landmarks, the true hypothesis is ultimately scored below zero and so removed. In other cases, a robot can temporarily get lost if there are locally gathered unregistered landmarks. Future work involves dealing with these exceptional cases in order to make a best guess on a true pose within the given map in spite of difficult situations.

## REFERENCES


[1] F. Aghili and A. Salerno, "Driftless 3-D attitude determination and positioning of mobile robots by integration of IMU with two RTK GPSs," *IEEE/ASME Trans. Mechatronics*, vol. 18, no. 1, pp. 21–31, Feb. 2013.

[2] I. Cox, G. Wilfong, R. Smith, M. Self, and P. Cheeseman, "Estimating uncertain spatial relationships in robotics," in *Autonomous Robot Vehicles*. New York, NY, USA: Springer, 1990, pp. 167–193.

[3] K. Tanaka, H. Ohtake, M. Tanaka, and H. O. Wang, "Wireless vision-based stabilization of indoor microhelicopter," *IEEE/ASME Trans. Mechatronics*, vol. 17, no. 3, pp. 519–524, Jun. 2012.

[4] H. Bay, T. Tuytelaars, and L. Van Gool, "SURF: Speeded up robust features," in *Proc. Comput. Vision ECCV*, 2006, pp. 404–417.

[5] M. Lourenco, J. P. Barreto, and F. Vasconcelos, "sRD-SIFT: Keypoint detection and matching in images with radial distortion," *IEEE Trans. Robot.*, vol. 28, no. 3, pp. 752–760, Jun. 2012.

[6] D. G. Lowe, "Distinctive image features from scale-invariant keypoints," *Int. J. Comput. Vision*, vol. 60, pp. 91–110, 2004.

[7] Y. Pang, W. Li, Y. Yuan, and J. Pan, "Fully affine invariant SURF for image matching," *Neurocomputing*, vol. 85, pp. 6–10, 2012.

[8] C. Cadena, D. Galvez-López, J. D. Tardos, and J. Neira, "Robust place recognition with stereo sequences," *IEEE Trans. Robot.*, vol. 28, no. 4, pp. 871–885, Aug. 2012.

[9] F. M. Campos, L. Correia, and J. M. F. Calado, "Global localization with non-quantized local image features," *Robot. Auton. Syst.*, vol. 60, pp. 1011–1020, 2012.

[10] T. Nicosevici and R. Garcia, "Automatic visual bag-of-words for online robot navigation and mapping," *IEEE Trans. Robot.*, vol. 28, no. 4, pp. 886–898, Aug. 2012.

[11] B. Bacca, J. Salvi, and X. Cufi, "Appearance-based mapping and localization for mobile robots using a feature stability histogram," *Robot. Auton. Syst.*, vol. 59, pp. 840–857, Oct. 2011.

[12] A. Kawewong, N. Tongprasit, S. Tangruamsub, and O. Hasegawa, "Online and incremental appearance-based SLAM in highly dynamic environments," *Int. J. Robot. Res.*, vol. 30, pp. 33–55, Jan. 2011.

[13] B. Qin, Z. J. Chong, T. Bandyopadhyay, M. H. Ang, Jr., E. Frazzoli, and D. Rus, "Curb-intersection feature based Monte Carlo localization on urban roads," in *Proc. IEEE Int. Conf. Robot. Autom.*, 2012, pp. 2640–2646.

[14] T. B. Kwon, J. H. Yang, J. B. Song, and W. Chung, "Efficiency improvement in Monte Carlo localization through topological information," in *Proc. IEEE Int. Conf. Intell. Robots Syst.*, Beijing, China, 2006, pp. 424–429.

[15] K. O. Arras, J. A. Castellanos, M. Schilt, and R. Siegwart, "Feature-based multi-hypothesis localization and tracking using geometric constraints," *Robot. Auton. Syst.*, vol. 44, pp. 41–53, Jul. 2003.

[16] T. He and S. Hirose, "A global localization approach based on line-segment relation matching technique," *Robot. Auton. Syst.*, vol. 60, pp. 95–112, Jan. 2011.

[17] F. Martin, L. Moreno, S. Garrido, and D. Blanco, "High-accuracy global localization filter for three-dimensional environments," *Robotica*, vol. 30, pp. 363–378, May 2012.

[18] A. Kar, "Linear-time robot localization and pose tracking using matching signatures," *Robot. Auton. Syst.*, vol. 60, pp. 296–308, 2012.

[19] H. Choi, D. Y. Kim, J. P. Hwang, C. W. Park, and E. Kim, "Efficient simultaneous localization and mapping based on ceiling-view: Ceiling boundary feature map approach," *Adv. Robot.*, vol. 26, pp. 653–671, 2012.

[20] H. Choi, E. Kim, Y. W. Park, and C. H. Kim, "Multiple hypothesis tracking for mobile robot localizaiton," in *Proc. SICE Annu. Conf.*, 2012, pp. 1574–1578.

[21] S. Thrun, W. Burgard, and D. Fox, *Probabilistic Robotics*. Cambridge, MA, USA: MIT Press, 2005.

[22] S. Thrun, D. Fox, W. Burgard, and F. Dellaert, "Robust Monte Carlo localization for mobile robots," *Artif. Intell.*, vol. 128, pp. 99–141, May 2001.

[23] H. Choi, S. Jo, and E. Kim, "CV-SLAM using line and point features," in *Proc. 12th Int. Conf. Control, Autom. Syst.*, 2012, pp. 1465–1468.


**Hyukdoo Choi** received the bachelor's degree in electrical and electronic engineering in 2009 from Yonsei University, Seoul, Korea, where he is currently working toward the Ph.D. degree in electrical and electronic engineering.

His current research interests include mobile robotics and simultaneous localization and mapping (SLAM).

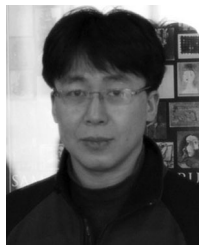

**KwangWoong Yang** received the Master's degree in automation engineering from Inha University, Incheon, Korea, in 1998.

He is currently with the Division of Applied Robot Technology R&D Group, Korea Institute of Industrial Technology (KITECH), Ansan, Korea. His current research interests include unmanned vehicles, 3-D object recognition, and simultaneous localization and mapping (SLAM).

**Euntai Kim** was born in Seoul, Korea, in 1970. He received the B.S. degree (as the top of the university) and the M.S. and Ph.D. degrees in electronic engineering, all from Yonsei University, Seoul, Korea, in 1992, 1994, and 1999, respectively.

From 1999 to 2002, he was a Full-Time Lecturer in the Department of Control and Instrumentation Engineering, Hankyong National University, Kyonggi-do, Korea. Since 2002, he has been with the faculty of the School of Electrical and Electronic Engineering, Yonsei University, where he is currently a Professor. He was a Visiting Scholar at the University of Alberta, Edmonton, AB, Canada, in 2003, and also was a Visiting Researcher at the Berkeley Initiative in Soft Computing (BISC), University of California, Berkeley, CA, USA, in 2008. His current research interests include computational intelligence and statistical machine learning and their application to intelligent robotics, unmanned vehicles, and robot vision.